Research
Medical Additive Manufacturing—Review

Visible Light-Induced 3D Bioprinting Technologies and Corresponding Bioink Materials for Tissue Engineering: A Review

Zizhuo Zheng [a,b], David Eglin [c], Mauro Alini [c], Geoff R. Richards [c], Ling Qin [a,d], Yuxiao Lai [a,b,e,*]

[a] Centre for Translational Medicine Research and Development, Shenzhen Institutes of Advanced Technology, Chinese Academy of Sciences, Shenzhen 518055, China
[b] Key Laboratory of Health Informatics, Shenzhen Institutes of Advanced Technology, Chinese Academy of Sciences, Shenzhen 518055, China
[c] AO Research Institute, Davos CH-7270, Switzerland
[d] Musculoskeletal Research Laboratory, Department of Orthopedics and Traumatology, The Chinese University of Hong Kong, Hong Kong 999077, China
[e] Guangdong Engineering Laboratory of Biomaterials Additive Manufacturing, Shenzhen 518055, China

ARTICLE INFO

ABSTRACT

Three-dimensional (3D) bioprinting based on traditional 3D printing is an emerging technology that is used to precisely assemble biocompatible materials and cells or bioactive factors into advanced tissue engineering solutions. Similar technology, particularly photo-cured bioprinting strategies, plays an important role in the field of tissue engineering research. The successful implementation of 3D bioprinting is based on the properties of photopolymerized materials. Photocrosslinkable hydrogel is an attractive biomaterial that is polymerized rapidly and enables process control in space and time. Photopolymerization is frequently initiated by ultraviolet (UV) or visible light. However, UV light may cause cell damage and thereby, affect cell viability. Thus, visible light is considered to be more biocompatible than UV light for bioprinting. In this review, we provide an overview of photo curing-based bioprinting technologies, and describe a visible light crosslinkable bioink, including its crosslinking mechanisms, types of visible light initiator, and biomedical applications. We also discuss existing challenges and prospects of visible light-induced 3D bioprinting devices and hydrogels in biomedical areas.

1. Introduction

With an alarming increase in the incidence of end-stage failure of vital organs, there is an urgent need for an innovative therapeutic approach that could effectively repair and restore damaged organs. In addition, the shortage of organs from optimal donors and matching difficulty are challenges confronting the field of organ transplantation. Recent notable achievements in tissue engineering for regenerating damaged tissue have gained considerable attention among transplant clinicians and researchers. Tissue engineering is recognized as a possible means to address the increasing demand for living organs and the limitations of living organs [1–4]. Cells, scaffolds, and biological/biochemical factors are generally referred to as essential elements of the "building blocks" of tissue engineering-based regenerative medicine strategies [5–7]. An ideal

bioactive scaffold for tissue engineering would provide a platform to support the interaction among cells, bioactive factors, and surrounding tissue [4]. In addition, scaffolds provide the physical support for cells and control the release of factors.

Charles W. Hull first proposed the concept of 3D printing technologies in 1986 [8]. Three-dimensional (3D) printing is a manufacturing process for constructing objects from computer-aided design models [5]. In contrast to traditional manufacturing, for example, casting and forging processes, 3D printing produces an object or scaffold by adding materials layer by layer and is one of the additive manufacturing technologies [1,3,5]. Bioprinting is becoming an increasingly attractive technology for designing ① the microstructure of scaffolds and control cells and ② the distribution of bioactive factors, and thereby, fulfilling the demand for regenerated tissues. The printing material, cell, and printing equipment/method are considered the most important factors in the application of this technology.

According to the American Society for Testing and Materials standard (F2792), 3D printing technologies are classified into

photopolymerization, material jetting, material extrusion, powder bed fusion, binder jetting, sheet lamination, and direct energy deposition [9]. In terms of cell viability and printing capability, the printing methods based on photopolymerization exhibit many advantages over other types of bioprinting methods, such as rapid curing at room temperature, high printing fidelity, and gentle reaction process. The printing structure and speed can be controlled conveniently by adjusting the light intensity, exposure time, and illuminated area [7]. Four out of the various bioprinting methods are widely applied to photo-cured bioprinting: inkjet, extrusion, stereolithography, and digital light process.

A bioink is a printing precursor in bioprinting and is typically based on thermosensitive or photopolymerization materials that contain cells [10]. It functions as a cell carrier, ensures precise positioning, and plays an important role in the protection of the cells during the printing process and that of the microenvironment formed by the material after printing. Among the many printing materials, hydrogel is a class of 3D network polymers formed through chemical bonds or physical forces. These can swell in water, but not dissolve in it. A few hydrogels display a permeable structure that is similar to the natural extracellular matrix (ECM). This structure provides a remarkable 3D microenvironment for cell proliferation [11–15]. Given these properties, many types of hydrogels can be applied to various areas of tissue engineering. Two types of crosslinking occur between polymer chains: chemical and physical crosslinking. The various crosslinking schemes affect the gelation kinetics and properties of hydrogels differently. Physically crosslinked hydrogels rely mostly on intermolecular van der Waals forces, hydrogen bonds, and other weak interaction forces. Chemically crosslinked hydrogels are formed by covalent bonds and are relatively stronger than physically crosslinked hydrogels [11]. Among the chemical crosslinking methods, photopolymerization has attracted considerable attention owing to its unique characteristics [16–18].

Photopolymerization is a simple, clean, and convenient method for achieving covalently crosslinked hydrogels. Photopolymerization can effectively control the formation and structure of hydrogels spatially and temporally. At present, photopolymerization is implemented largely using ultraviolet (UV) light. This may cause cell damage during exposure [19]. In contrast, when UV light is replaced with visible light, the hydrogel system achieves higher cell compatibility and wider application prospects. In addition, visible light has a higher penetration depth, which results in a more uniform hydrogel structure [20]. Visible light crosslinkable hydrogels have been widely researched and applied in many fields such as tissue engineering [21], 3D cell encapsulation [22], and drug delivery [23].

In this review, we briefly discuss the operating principles and specialities of 3D bioprinting technologies and devices that can be applied to visible light-induced bioprinting systems (Table 1 [20,21,24–33]). Then, we systematically summarize visible light crosslinkable bioink, including the crosslinking mechanisms and visible light initiators, and highlight their biomedical applications. Finally, existing challenges in the bioprinting and visible light crosslinkable hydrogels are discussed, and future prospects and development directions are proposed.

2. Photo-induced 3D bioprinting methods

2.1. Inkjet-based bioprinting

Inkjet-based bioprinting originated from commercial 2D inkjet printing, which drops and deposits a cell-laden bioink into a predefined area to form a preset shape [34]. The droplet, which is ejected from the nozzle to the substrate, is typically produced via thermal or piezoelectric actuation, as shown in Fig. 1 [24]. Thermal actuation generates droplets through heating elements that overheat the bioink in 2 µs, such that a high temperature (e.g., 300 °C) will not affect cell viability [9]. Piezoelectric actuation adjusts the voltage rapidly to force the bioink to expel a droplet through the piezoelectric material. The gelation of bioink by physical and chemical processes can occur simultaneously with the printing process to guarantee printing fidelity. With the low volume of droplets (10–50 µm in diameter) and high throughput (up to 10 000 droplets per minite), inkjet-based printing ensures a high printing resolution (lower than 50 µm) and printing speed [24]. In addition, the cell viability after printing can exceed 80%. However, a drawback of inkjet-based bioprinting is that its application is limited to low-viscosity bioink because a high viscosity bioink tends to clog the nozzle and cause high shear stress [35]. Consequently, inkjet-based bioprinting limits the options of bioink materials and cell concentrations. Furthermore, it is challenging to form large and complex 3D structures. Acosta-Vélez et al. [25] developed a drug tablet that can be fabricated in 30 s by inkjet printing under exposure to visible light. The visible light system was used rather than UV because the latter affects drug stability [25].

2.2. Extrusion-based bioprinting

Extrusion-based printing is one of the most common additive manufacturing methods used for fabricating scaffolds. The extrusion is controlled by pneumatic, piston-driven, and screw-driven systems [36]. Unlike the case of inkjet-based printing, the pressure of the extrusion process can be conveniently controlled, and the viscosity of bioink can be within a wider range (30–6 × 10⁷ MPa·s). That is, the selection of materials can be more diverse, albeit with limitation in terms of viable cell support [37]. In accordance with the fundamental theory of the extrusion process, the major drawback of extrusion-based printing is the limited resolution and low printing speed, because of the size of the needles. The resolution of extrusion printing by current bioprinting applications can attain

Table 1
Visible light-induced bioprinting methods.

Method	Printing speed	Resolution	Vertical structure	Advantage	Limitation	Application	Cell viability
Inkjet	Fast	50 µm	Poor [24]	Support low viscosity bioink	Only low viscosity inks, poor vertical printing ability	Drug delivery [25,29], cell patterning [21]	> 80% [21]
Extrusion	Slow	≥ 100 µm	Good [24]	Simple, easy, suitable for a variety of hydrogels	Relatively low cell viability	Bone [30], 3D cell embedding [31]	40%–95% [31,32]
SLA	Fast	50 µm [26]	Good [24]	Nozzle free, no limitation in ink viscosity, high efficiency	Not support multi-cells structure	Tube construct [33]	> 85% [33]
DLP	Fast	50 µm [27]	Good [24]	Nozzle free, no limitation in ink viscosity, high efficiency [28]	Not support multi-cells structure	Skin [24], bone and cartilage [20], complex model printing [28]	> 90% [20]

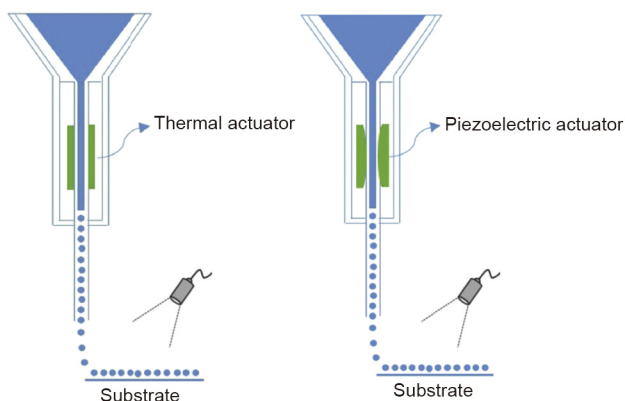SLA: stereolithography; DLP: digital light processing.

Fig. 1. Schematic diagram of inkjet-based bioprinting. Reproduced from Ref. [24] with permission of Elsevier, © 2018.

100 μm [9]. The location of the optical device becomes critical when a photocrosslinkable bioink is applied to extrusion-based bioprinting. The photocuring process could be performed before (pre-crosslink), after (post-crosslink), or during (*in-situ*-crosslink) extrusion, as shown in Fig. 2 [38]. Ouyang et al. [38] illustrated that pre-crosslinking resulted in high and inconsistent extrusion forces, heterogeneous printed structures, and low cell viability (about 47%). Although post-crosslinking could improve the cell viability and lower the extrusion force, the bioink flowed prior to stabilization and could not maintain the filament structure. The hydrogel could crosslink before deposition (*in-situ*-crosslink with UV or visible light) when the needle was replaced with a photo-permeable capillary. This yielded a high printing fidelity and relatively high cell viability (over 95%) after printing [38]. Through adjustments of the hydrogel concentrations, post-crosslink could achieve higher fidelity under visible light than under UV in extrusion-based bioprinting, and also ensure a high cell viability (over 90%) [39].

2.3. Stereolithography and digital light process

Stereolithography (SLA) and digital light processing (DLP) have similar molding mechanisms.

SLA is one of the printing methods that use digital micromirror arrays to control the light intensity of each pixel for the printing areas [6]. During SLA printing, a laser light is applied to a liquid photosensitive material in a point-by-point manner to form a solidified layer. After the solidification of the first layer, the platform rises by a defined height, and a second layer is photocrosslinked. This is repeated until the complete shape is printed (Fig. 3(a)). SLA does not require extrusion through a nozzle and is faster, more accurate, and has a higher resolution (< 100 μm) than extrusion-based printing [40]. In general, SLA bioprinting uses UV light as its light source. It induces cell damage during bioprinting, thereby limiting its use. Wang et al. [26] developed a visible light-induced SLA-based bioprinting process and used it with an eosin Y (EY)-based photoinitiator to fabricate a polyethylene glycol diacrylate (PEGDA) and gelatin methacrylate (GelMA) composite hydrogel. They achieved a resolution of 50 μm and high cell viability (85%) for at least five days [26].

DLP bioprinting is similar to the SLA-based printing method, except that it uses a projector to project light onto photopolymerized materials for curing the layer image rather than a point [41–43] (Fig. 3(b)). The print speed of DLP is higher than that of SLA, particularly when printing larger objects. However, the printable area is reduced in comparison with that of SLA because of the constraints imposed by the project area and resolution of the digital light mirrors. Consequently, only small objects are generally printed. Lim et al. [39] explored the resolution of 3D DLP printing of silk fibroin (SF) hydrogel. They attained a resolution of 66 μm in the *X*-direction and 146 μm in the *Z*-direction. This indicates its capability of printing complex structures (e.g., Eiffel Tower) with high precision [39]. Lim et al. [39] developed a visible light-induced DLP system. It achieved a resolution of 50 μm and cell viability of over 90% [27]. DLP is a highly efficient method of layer-by-layer printing. Kelly et al. [44] presented a new method for manufacturing by rotating a photopolymer in a dynamically evolving
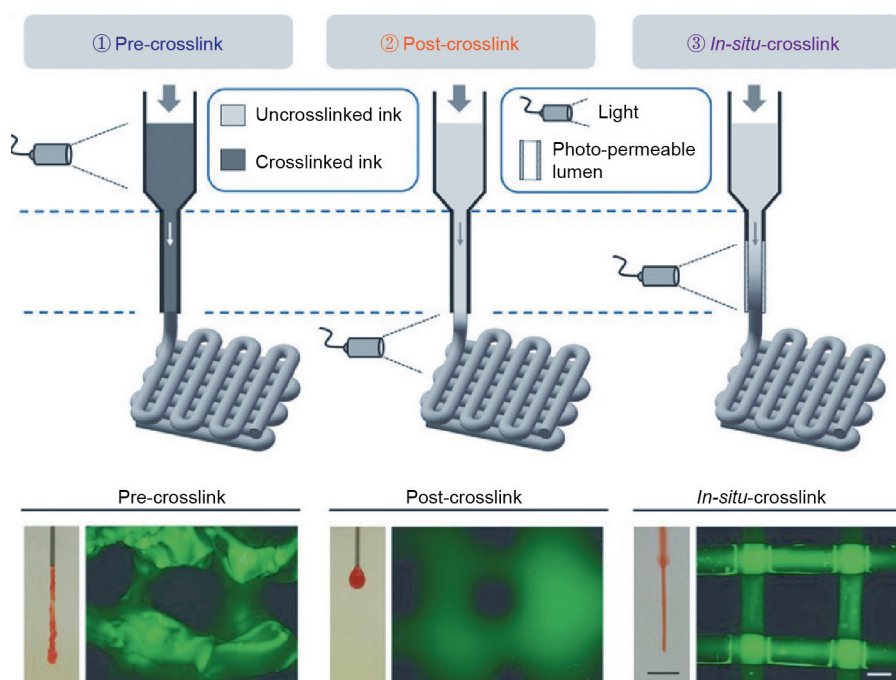

Fig. 2. Schematic diagram of three extrusion-based bioprinting. Reproduced from Ref. [38] with permission of Wiley, © 2017.
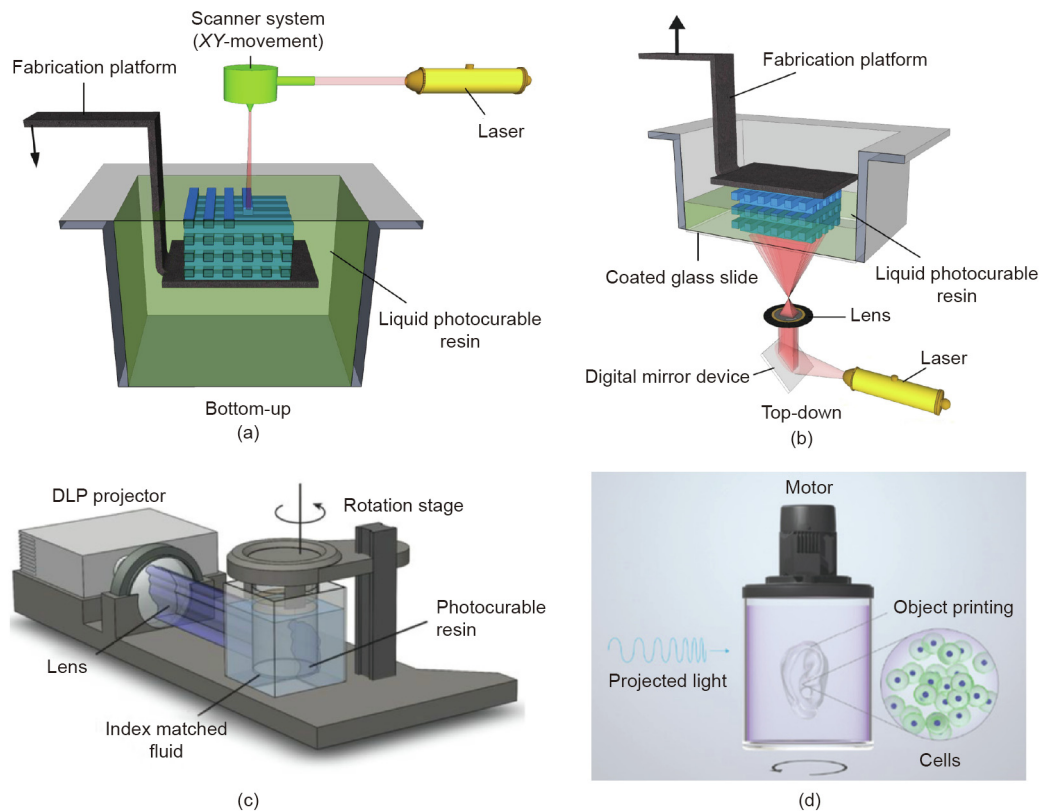
Fig. 3. Schematic diagram of (a) SLA and (b) DLP bioprinting method. (c) Schematic of the computed axial lithography system. (d) Volumetric bioprinting process showing the cell-laden gel-resin reservoir connected to a rotating platform. (a, b) Reproduced from Ref. [10] with permission of Elsevier, © 2012; (c) reproduced from Ref. [44] with permission of Science, © 2019; (d) reproduced from Ref. [28] with permission of Wiley, © 2019.

light field (Fig. 3(c)). It is based on the DLP method. This method is scalable to larger print volumes and is faster by several orders of magnitude than the common DLP method, under a wider range of conditions [44]. Bernal et al. [28] used visible light (405 nm)-induced volumetric bioprinting (Fig. 3(d)) to print complex centimeter-scale architectures (including anatomically correct trabecular bone models with embedded angiogenic sprouts and meniscal grafts). They achieved a high cell viability (> 85%) in seconds to tens of seconds [28]. These methods are summarized in Table 1.

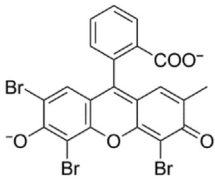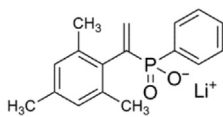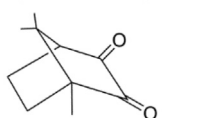## 3. Visible light crosslinkable materials
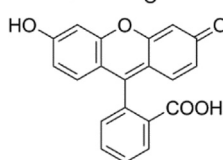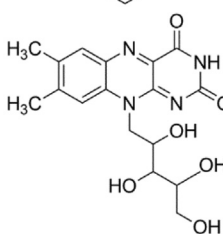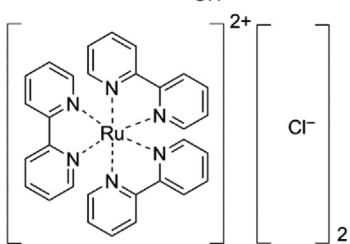
3.1. Visible light initiators

Most of the photocrosslinkable bioinks require the presence of photoinitiators. The type of photoinitiator and the duration of exposure to visible light can affect the cell viability and photoinitiation efficiency. Therefore, the selection of a visible light initiator requires the consideration of its absorption spectrum, water solubility, capability to generate free radicals, and stability.

Visible light initiators can be classified into free radical and cationic photoinitiators based on the polymerized active species. However, cationic photoinitiators cannot be applied in the biomedical field because of the protonic acid produced when polymerization is initiated [7,16]. Therefore, visible light crosslinkable hydrogels rely mostly on visible light-initiated radical polymerization. Free radical photoinitiators can be divided into type I (one-component pyrolysis) and type II (photosensitizer/co-initiator photoinitiators) [45]. Type I photoinitiators absorb incident photons and divide them into two primary radicals upon exposure to

light. However, less options are available in the visible region for a type I photoinitiator, and lithium phenyl-2,4,6-trimethylbenzoyl phosphinate (LAP) is commonly used [46]. In contrast, there are considerably more and diverse alternatives for type II photoinitiators, which extract hydrogen from the co-initiator to generate secondary radicals. At present, the ruthenium pyridine complex, EY, and camphorquinone (CQ) are attracting significant attention and being widely applied in tissue engineering. In a visible light crosslinkable hydrogel system, the cytotoxicity and absorption spectrum of the initiator are particularly important for the encapsulated cells. The commonly used visible light initiators are listed in Table 2 [39,46–56].

The CyQuant Direct Cell Proliferation Assay method reveals that the viability of human primary renal proximal tubule epithelial cells (hRPTECs) decreases marginally as the LAP concentration increases. However, it can still satisfy the biocompatibility standard [51]. In an early work, Lin et al. [57] introduced LAP-initiated GelMA hydrogel-encapsulated human bone marrow-derived mesenchymal stem cells (MSCs) that exhibit long-term viability and proliferation (over 90 d) and good integrity. Although LAP can absorb the energy of near-UV blue light (405 nm) to produce free radicals, the cost of producing a bioprinting device with a similar blue light is high. Moreover, this type of device is not remarkably superior to the current UV bioprinting system. Furthermore, such strong near-UV blue light is hazardous to mammalian cells and disruptive to cellular processes [51]. CQ, fluorescein, and riboflavin (RF) have similar absorption spectra (between 400 and 500 nm) [52]. The methacrylated glycol chitosan (MeGC) hydrogels initiated by these types of initiators are tested. The results show that the hydrogel initiated by RF has the highest mechanical strength and lowest cytotoxicity. Moreover, the

Table 2
Types of visible light initiators.

Name	Structure	Absorption spectrum (nm)	Materials	Encapsulated cells	Cell viability	References
EY		515	PEGDA	3T3 fibroblasts	> 96%	[47]
			HA-Tyr	hMSC	> 96%	[48]
LAP		365/405	PEGDA	Human neonatal fibroblasts	95% (1 d)	[49,50]
			GelMA	Human articular chondrocytes	70% (1 d)	[46]
			GelMA	Human primary renal proximal tubule epithelial cells	> 90%	[51]
CQ		450	MeHA	Human bone sarcoma cells	> 85% (1 d)	[52,53]
FR		~490	MeGC	Primary articular chondrocytes	~80%	[52]
RF		444	HA-Tyr	T/C-28a2 chondrocytes	99% (1 d)	[52,54]
$[Ru(II)(bpy)_3]^{2+}$		452	Gtn-HPA	Kidney cells	~90%	[55,56]
			GelMA	Breast adenocarcinoma cells	> 85% (21 d)	[39]

FR: fluorescein; RF: riboflavin; HA-Tyr: hyaluronic acid-tyramine; MeHA: methacrylated hyaluronic acid; MeGC: methacrylated glycol chitosan; Gtn-HPA: gelatin-hydroxy-phenylpropionic acid; hMSC: human marrow stromal cell. $[Ru(II)(bpy)_3]^{2+}$: tris(2,2′-bipyridyl)dichlororuthenium(II) hexahydrate.

gelation time and cell exhibit a negative correlation [52]. Donnelly et al. [54] developed an RF-initiated tyramine-substituted hyaluronate (HA-Tyr) hydrogel to coat TC-28a2 chondrocytes. It showed over 99% cells to be alive after one day.

Among visible light initiators, EY has many more advantages than others [2]. EY is highly water-soluble, and has an absorption peak at approximately 515 nm and low cytotoxicity [51]. EY and LAP exhibit a similar cytocompatibility for hepatic progenitor HepaRG cells. It is noteworthy that in contrast to LAP, the gelatin hydrogel initiated by EY marginally increases the degree of hepatic gene expression [58]. Gwon et al. [59] demonstrated that human adipose-derived MSCs grow and proliferate effectively in hyaluronic acid (HA) hydrogel mortified with heparin (cell viability of 95%). Furthermore, the hydrogel can support 3D adipogenic differentiation of adipose-derived MSCs [59]. Kerscher et al. [60] demonstrated that low-density GelMA hydrogels can be formed in 1 min by EY and that they facilitate high efficiency cardiac differentiation. On Day 8 of differentiation, the hydrogel initiated spontaneous contractions in conjunction with synchronicity, frequency, velocity, and appropriate temporal variations in the cardiac gene expression [60].

The tris(2,2′-bipyridyl)dichlororuthenium(II) hexahydrate ($[Ru(II)(bpy)_3]^{2+}$)/sodium persulfate (SPS) system also displays unique strength. $[Ru(II)(bpy)_3]^{2+}$/SPS can alleviate the effect of oxygen inhibition during the polymerization, which affects the fidelity of 3D bioprinting in the vertical direction [39]. 3D bioprinting is widely adopted for printing complex structures that are to be implanted *in vivo*, wherein it is challenging to maintain the structure in the vertical direction and ensure precision in the horizontal direction. A few studies have revealed that the print fidelity of 3D bioprinting and the photopolymerized hydrogel structure are directly affected by oxygen inhibition. The presence of oxygen affects free radicals because these can react with oxygen and be converted into peroxyl radicals, which cannot react with unsaturated bonds. Meanwhile, peroxyl radicals reduce the number of protons in the system. This results in the formation of either hydroperoxides or alcohols that hinder the formation of covalent crosslinks. These reactions cause an incomplete or insufficient

formation of hydrogels, thereby affecting the stack between layers and the printing fidelity in the vertical direction. To solve this problem, Lim et al. [39] applied the visible light + [Ru(II)(bpy)$_3$]$^{2+}$/SPS system. Unlike the UV + I2959 system, this system alleviates the effects of oxygen inhibition on porous biofabricated constructs (Fig. 4 [61]) and maintains a cell viability of over 85% in 21 d [39]. Al-Abboodi et al. [55] developed a gelatin-hydroxyphenylpropionic acid (Gtn-HPA) conjugate hydrogel initiated by [Ru(II)(bpy)$_3$]$^{2+}$/SPS. It shows good cell viability (over 85%).

3.2. Mechanisms of photopolymerization and gelation

There are two types of photopolymerization: photoinitiator-free polymerization and photoinitiator polymerization. Photoinitiator-free polymerization is directly initiated by UV light. Farkas et al. [6] developed a type of photoinitiator-free 3D scaffold. It is fabricated by excimer laser photocuring under light with a wavelength of 248 or 308 nm [6]. It shows higher cell viability than those initiated by photoinitiators. However, this type of polymerization requires energy higher than that of the covalent bond of the monomer. Furthermore, it is challenging to satisfy this requirement in the visible range. Therefore, it is unlikely to be applied in the field of visible light-induced polymerization. Polymerization under visible light requires an initiator. Three types of gel mechanisms have been widely used in studies: free radical-initiated chain polymerization, thiol–ene "click" reaction, and photo radical coupling reaction. The details of the gelation mechanisms are described below.

3.2.1. Free radical-initiated chain polymerization

The development and advancement of synthetic chemistry has enabled the modification and synthesis of functionalized monomers and macromolecular chains through various methods. Furthermore, photocrosslinkable bioinks can be prepared through free-radical polymerization (FRP). The process of FRP has three reaction stages, as shown in Fig. 5: chain initiation, propagation, and termination [14]. After a radical is generated via the exposure of an initiator to light, the radical reacts with a double bond to generate a new radical. This reacts further with a double bond on the monomer or forms oligomers, and propagates further until termination [7].

Owing to the cytoxicity of the methacrylate monomers, bioinks amenable to FRP are produced by introducing a limited amount of methacryloyl groups using methacrylic anhydride [62], glycerol methacrylate [63], or methacryloyl chloride [24], into natural or synthetic macromolecular chains, and then selecting a suitable photoinitiators to produce water-based photocrosslinkable bioinks. The mechanisms of FRP and gelation are illustrated in Fig. 5.
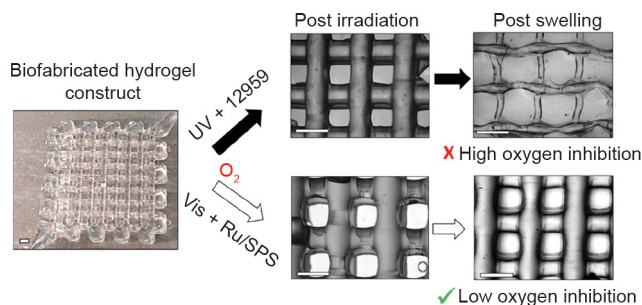

Fig. 4. Difference between UV- and visible light-polymerized GelMA/collagen constructs. Vis: visible light; Ru: [Ru(II)(bpy)$_3$]$^{2+}$. Reproduced from Ref. [61] with permission of American Chemical Society, © 2016.

3.2.2. Thiol–ene "click" reaction

The thiol–ene "click" reaction is a fast, highly selective, and versatile method for preparing photocrosslinkable hydrogels. Classical thiol–ene chemistry emerged when Charles Goodyear discovered the vulcanization of natural rubber (poly(cis-isoprene)) by sulfur in the mid-19th century. Since then, the mechanism, kinetic characteristics, and properties of sulfhydryl/vinyl polymerization have been studied extensively [64,65]. The radical growth mechanism of sulfhydryl/radical photopolymerization is different from the growth mechanism of the free radical chains of vinyl. Furthermore, the sulfhydryl monomers correspond to crosslinkers [65]. The thiol–ene reaction is unaffected by oxygen inhibition in air and can achieve photopolymerization rapidly [66,67]. Therefore, a lesser amount of photoinitiator is used. Furthermore, the formation of thioether bonds can enhance the strength of materials.

After the initiator is activated, protons are abstracted from sulfhydryl groups to form thiyl radicals. These then react with vinyl bonds. The reaction forms a thioether bond and another carbon-centered radical that can generate another thiyl radical. The thiol–ene reaction propagates until the limiting moiety is depleted [64]. The reaction with an electron-rich vinyl monomer such as norbornene [68], acrylate, methacrylate, styrene, or conjugated diene [13,40] involves the homopolymerization reaction of vinyl monomers and the copolymerization reaction between the thiol and vinyl groups [65] (Fig. 6).

3.2.3. Photo radical coupling reaction

This type of reaction generally requires the presence of phenolic hydroxyl groups such as Tyr. Furthermore, ruthenium (Ru(II)) or EY is commonly used as the visible light initiator. Different initiators display different initiation mechanism during the reaction. [Ru(II)(bpy)$_3$]$^{2+}$ is photo-oxidized into [Ru(III)(bpy)$_3$]$^{3+}$ by visible light. Then, the activated Ru(III) extracts an electron from the phenolic hydroxyl group (Fig. 7(a)). This yields a radical species that can then attack a wide variety of other groups [69], as shown in Fig. 7(b). However, the ground-state EY absorbs a photon is transformed to the first excited singlet state (^{1}EO). It is then converted to a long-lived triplet state (^{3}EO*) by intersystem crossing. Energy is transferred in the presence of oxygen to form singlet oxygen (^{1}O$_2$) [70]. Then, the singlet oxygen reacts with phenolic hydroxyl groups to yield radical species that sustain the crosslinking, as
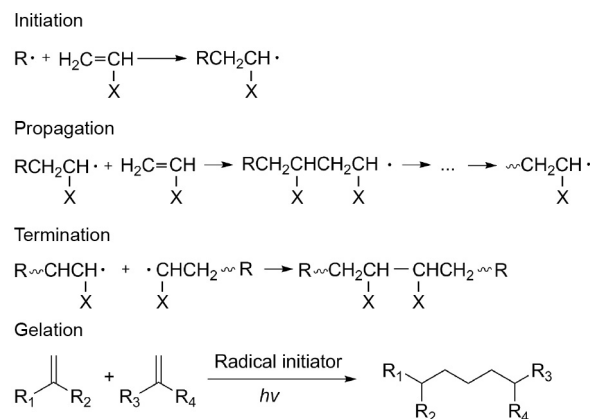

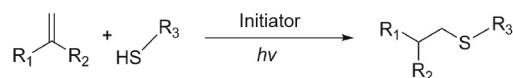**Fig. 5.** Mechanism of FRP and gelation. hv: photon energy.

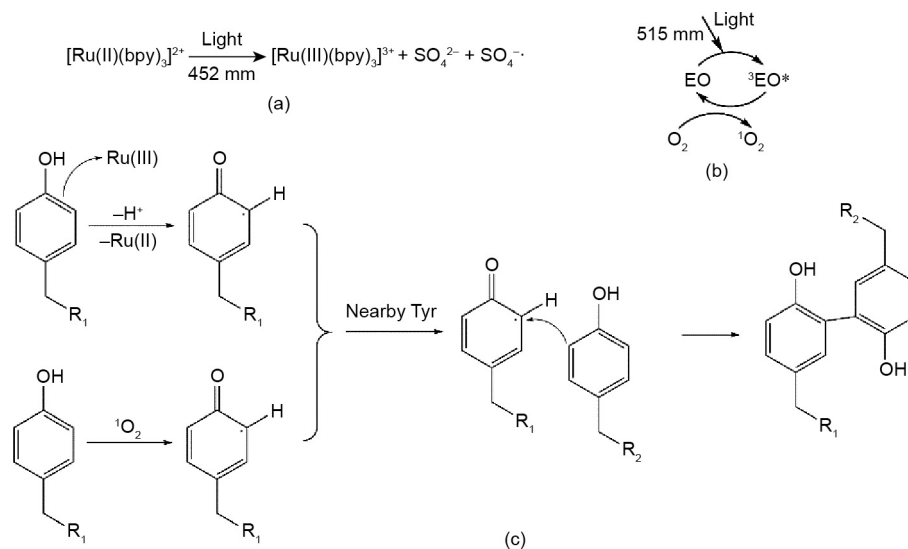**Fig. 6.** Mechanism of thiol–ene "click" reaction. hv: photon energy.

Fig. 7. The mechanism of photo radical coupling reaction. (a) Initiation mechanism of ruthenium; (b) initiation mechanism of EY; (c) the mechanism of photo radical coupling reaction.

shown in Fig. 7(c). The commonly used strategy to achieve this reaction is to modify the polymer with molecules containing a phenolic hydroxyl group. Sakai et al. [33] successfully developed a type of bioink by modifying alginate with TYR. This ink could be gelled using a normal desktop lamp in 10 s [33].

3.3. Visible light crosslinkable materials

Photopolymerized materials are primarily categorized into nature-derived and synthetic materials. The most common method to achieve photopolymerization capability is to modify the specific side or terminal groups with compounds that contain a double bond, such as acrylate, methacrylate, styrene, conjugated diene, and Tyr. The common types of photopolymerized materials and modified methods are provided in Table 3 [23,27,33,46,51,55,71–85].

3.3.1. Nature-derived materials

Cells are reportedly incubated in the ECM, which is made up of complex structural and functional macromolecules. Natural materials are derived from organisms' polysaccharides and proteins. Most of the nature-derived materials such as gelatin and collagen have superior cell response and cell adhesion, and can be degraded *in vivo*. In addition, nature-derived materials are inexpensive and renewable. However, these have a few limitations, for example, high degradation rate, complex purification process, and poor mechanical properties.

Gelatin is an animal protein that is isolated from animal tissues and prepared through the thermal denaturation of collagen [6,85], which is a heterogeneous aggregation of polypeptides that contain 18 amino acids [86]. Considering the gelatin construct, gelatin exhibits the potential to be modified with functional monomers without a significant reduction in its cytocompatibility. Lin et al. [85] introduced degradable gelatin hydrogel-encapsulated human bone marrow-derived MSCs. They exhibit long-term viability and proliferation (over 90 d) and good integrity. In 2000, Van Den Bulcke et al. [87] first developed and patented the photopolymerizable gelatin methacryloyl derivative, GelMA. It was obtained through the reaction of primary amines in the side chains of (hydroxy)-lysine and ornithine and methacrylic anhydride [47,48]. The GelMA precursor forms hydrogen bonds between the chains at a low temperature (< 25 °C) to increase the solution's viscosity. This facilitates the attainment of the 3D printing process' viscosity requirement. GelMA has been widely applied for bioprinting either as a standalone material or by being co-crosslinked with other materials to form a hydrogel. Several types of photocrosslinkable gelatin derivatives based on this conjugation method have been developed in addition to GelMA. Mazaki et al. [71] developed a furfurylamine-conjugated gelatin. It could crosslink by visible light, thereby supporting bone marrow-derived stromal cells chondrogenic differentiation *in vitro* [71].

Chitosan is a polysaccharide that consists of randomly distributed β-(1–4) linked D-glucosamine and N-acetyl-D-glucosamine. It is prepared from the chitin shells of shrimp and other crustaceans, through chemical processing [75]. Given its antifungal and antibacterial activities, chitosan has been approved by the US Food and Drug Administration (FDA) for medical wound dressing. With regard to its chemical properties, the presence of hydrogen bonds decreases chitosan's solubility in water [88]. The abundant groups in chitosan, such as amidogen, provide many opportunities for modifying region properties. Chitosan can be reacted with methacrylate anhydride or glyceryl methacrylate to form a photopolymerizable chitosan derivative. This derivative can be used for bioactive carriers [23,75] and bioink [89].

HA is a non-sulfated glycosaminoglycan with disaccharide unit repeats of D-glucuronic acid and N-acetyl-D-glucosamine [90,91]. HA is distributed widely in connective, epithelial, and neural tissues, typically in an anionic form. Each monomer of HA has sites for modification with reactive groups [92]. Therefore, researchers have refined existing chemistries for synthesizing HA macromer derivatives such as methacryloyl HA [38] and norbornene functionalized HA [77]. With regard to its roles in the ECM, HA exhibits high hydrophilicity and considerable cytocompatibility to support cell growth, migration, and differentiation [91]. Gwon et al. [59] demonstrated that human adipose-derived MSCs grow and proliferate well in HA hydrogel mortified with heparin. The production of several types of functional marker and their synergistic effects could be observed during the cell culture [82]. Hinton et al. [93] used methacrylated HA (MeHA), collagen, and other soft materials to test a new extrusion-based bioprinting method (freeform reversible embedding of suspended hydrogels). It displayed substantial potential to be applied in bioprinting natural materials [93].

SF is an insoluble protein that is present in silk produced by silk worms. It has three chains: light, heavy, and glycoprotein P25

973

Table 3
Photopolymerized materials characteristics and applications.

Source	Material	Chemical structure	Characteristic	Application	References
Natural	Gelatin		GelMA	Kidney, cartilage	[46,51]
			Gelatin-FA	Cartilage	[71,72]
			Gtn-HPA	Skin	[55]
			Gel-NBGel-SH	Hepar	[73]
	Chitosan		MeGC	Skin	[23,74]
			Hpp-GC	Liver	[75]
	HA		MeHA	Cartilage, intervertebral disc	[76]
			NorHA	Cartilage	[77,78]
Natrual	SF		SFMA	Heart, vessel, brain, trachea, ear	[79]
	Alginate		Alg-Norb	Cartilage	[80]
			Alg-Ph	Cartilage	[81]
			NorPEG	Tube	[33]
Synthetic	PEG		PEGDA	Bone, cartilage	[82]
			PVAMA	Cartilage, tracheal tube	[83,84]
	PVA		Alg-Norb	Cartilage, bone	[27]

Gelatin-FA: furfurylamine-conjugated gelatin; Gel-NB: gelatin norbornene; Gel-SH: thiolated gelatin; Hpp-GC: chitosan 3-(4-hydroxyphenyl) propionic acid conjugate; MeHA: methacrylated hyaluronic acid; NorHA: norbornene functionalized hyaluronic acid; SFMA: methacrylated SF; Alg-Norb: norbornene functionalized alginate; Alg-Ph: phenolic hydroxyl functionalized alginate; PEG: polyethylene glycol; NorPEG: norbornene-terminated PEG; PVA: polyvinyl alcohol; PVAMA: methacrylated PVA; Ala: alanine; Gly: glycine; Pro: proline; Arg: arginine; Glu: glutamic acid; Hyp: hydroxyproline.

chains. The heavy and light chains are linked by disulfide bonds. Moreover, these associate with P25 via noncovalent interactions [94]. Given its nontoxicity, low immunogenicity, and low degradation rate [95], SF can be applied to wound dressing, enzyme immobilization matrix, vascular prosthesis, and structural implant [79]. SF is also applied to bioprinting after modification. Kim et al. [79] developed a modified glycidyl methacrylated SF bioink. It enabled the construction of highly complex organ structures including the heart, vessel, brain, trachea, and ear with remarkable structural stability and reliable biocompatibility [79].

Alginate is an anionic polysaccharide that consists of linear copolymers of β-(1–4) linked D-mannuronic acid and β-(1–4)-linked L-guluronic acid units obtained from brown seaweed [81]. Alginate's properties such as the superior biocompatibility, low toxicity, low cost, and convenient gelation ensure its applicability to bioprinting [96]. In general, the bioprinting process of alginate involves the addition of divalent cations (Ca^{2+}, etc.) [97]. However, the common alginate hydrogel lost these mechanical properties rapidly during in vitro culture (approximately 40% within nine days). Furthermore, they have inadequate cell adhesive sites [61]. If the carboxyl of an alginate monomer reacts with 2-aminoethyl methacrylate (AEMA), the methacrylated alginate could become photocrosslinkable and improve its mechanical properties [80]. Norbornene functionalized alginate enables printability at a lower concentration (2 wt%) and maintains a more stable 3D construct than pure ionic crosslinking printing [81].

3.3.2. Synthetic materials

Although synthetic materials have inadequate bioactivity compared with nature-derived materials, their chemical and mechanical properties are reproducible, consistent, and tunable owing to the control over the chemical and biological functional group presentation [15].

Polyethylene glycol (PEG), also called polyethylene oxide or polyoxyethylene, is a linear synthetic polyether of ethylene glycol, which is hydrophilic. The terminal functional groups of PEG and its highly controllable molecular weight enable the modification of the terminal functional groups [98] and its synthesis into four-arms [99] or eight-arms [100], thereby increasing the diversity of materials. The major advantages of the application of PEG to tissue engineering include the adjustable structure and mechanical properties, biocompatibility, hydrophilicity, low cytotoxicity, and non-immunogenicity [101]. Because PEG is nondegradable and has inadequate adhesion sites for cells, it is generally compounded with other materials or peptides to develop bioinks. Bal et al. [102] used several types of peptides to mortify PEG hydrogel (which is initiated by EY) to observe how the combination of MSCs and ligand in a hydrogel affects the insulin secretion of the pancreatic islets.

Polyvinyl alcohol (PVA) is a hydrophilic linear synthetic ethanol homopolymer. The large number of side hydroxyl groups provide the attachment sites for biomolecules and opportunity for modification. The hydrogels prepared from PVA and its derivatives are widely used because of these adjustable chemical properties [5]. Pure PVA hydrogel cannot afford long-term cell growth: The MSC cell viability decreases from 87% (Day 1) to 71% (Day 14). When it is combined with GelMA, the cell viability could be 92% on Day 14 [27].

3.4. Visible light-induced 3D bioprinting applications

3.4.1. Tissue engineering

3D bioprinting is primarily used for tissue engineering and regenerative medicine. The ultimate aim is to form artificial tissue substitutes and further, to construct artificial organs. However, at present, it is not possible to form a fully functional artificial tissue substitute to be used in vivo. Therefore, to achieve this ambitious goal, the leading research studies focus on fabricating models in vitro to mimic the in vivo conditions.

To achieve the fabrication of models in vitro, researchers require a high printing resolution to simulate the complex structures of tissues in vitro. Wang et al. [26] developed a visible light-induced SLA-based bioprinting system to prepare PEGDA and GelMA hydrogels with EY. The resolution of the vertical 3D structure was 50 μm (Fig. 8(a)), and the cell viability of NIH 3T3 fibroblast cells is 85% for at least five days [26]. The work of Bertlein et al. [56] demonstrated that the visible light + [Ru(II)(bpy)$_3$]$^{2+}$/SPS system has higher fidelity (Figs. 8(b) and (c)) and longer-term (three weeks) cell viability than the UV + I2959 system. Lim et al. [27] also developed a cell-laden methacrylated PVA (PVAMA)/GelMA bioink for DLP bioprinting. It enabled the bioprinting of complex structures with high resolutions (25–50 μm) (Fig. 8(d)). It also enabled the encapsulated cells to survive up to 90% in 14 d [27].

Apart from high resolution, it is important to also consider the state of cell proliferation, adhesion, and differentiation in printed construct. Wang et al. [103] also developed an EY/GelMA hydrogel system that forms a 3D cellular network inside the printed pattern on Day 5 (which reveals the potential benefits of the research on cell growth morphology), as shown in Fig. 9(a). Sakai et al. [33] revealed that Nanog, Oct-4, and Sox-2 genes were upregulated significantly (two- to three-fold from that on Day 1) after human adipose stem cells (hADSCs) were enclosed in tyrosinized HA/gelatin printing structure for 25 d. This indicated that the hADSCs maintained pluripotency [32]. Lim et al. [27] demonstrated that PVAMA/GelMA hydrogel supported the osteogenic and chondrogenic differentiation of MSCs. Ouyang et al. [38] reported a norbornene-modified HA hydrogel for coating MSCs. Furthermore, histological analyses validated the production of both glycosaminoghycan (GAG) and collagen (COL) by encapsulated MSCs after 56 d of chondrogenic culture [104]. Petta et al. [48] recently introduced a double crosslinkable hyaluronan bioink crosslinked through enzymes and visible light. It exhibited flexible shear-thinning properties under low substitution during extrusion-based bioprinting [48]. Moreover, it preserved the main structure and properties, thereby enabling human marrow stromal cells (hMSCs), chondrocytes, and human telomerase reverse transcriptase (hTERT) fibroblasts to be cultured and recover their 3D shape [20].

The fabrication of multilayer constructs consisting of different cells and material compositions is a key requirement for mimicking the skin structure. DLP bioprinting can form hydrogel-containing cells similar to the skin, layer by layer. Kwak et al. [105] developed SF/PEG composite hydrogel as an artificial skin model by visible light-induced DLP. Although it retained a high cell-survival rate in the early stages, a dense keratin layer formed on the hydrogel surface within six weeks, as shown in Fig. 9(b) [105].

The heart is one of the most important organs of humans. The complex structure and interaction of multiple cells determine its function. Kumar et al. [72] used furfuryl-gelatin and RF to print multilayered sheets containing C2C12 myoblasts and STO fibroblasts, to study the interaction between cardiac myocytes and fibroblasts in vivo. During the culture and incubation, the different layers combined together owing to their interaction at the junction, rather than falling apart (Fig. 9(c)) [72]. Kumar et al. [106] also developed a fibrin–gelatin bioink for coculturing and coupling of cardiomyocytes and cardiac fibroblasts. In addition, the immunochemistry data demonstrated the heterocellular coupling between two types of cells via connexin43 adhesion junctions, which is critical for cell interactions [106].

A fully functional artificial organ cannot live without a vascularized network. Bioprinting is an effective method for reconstruct
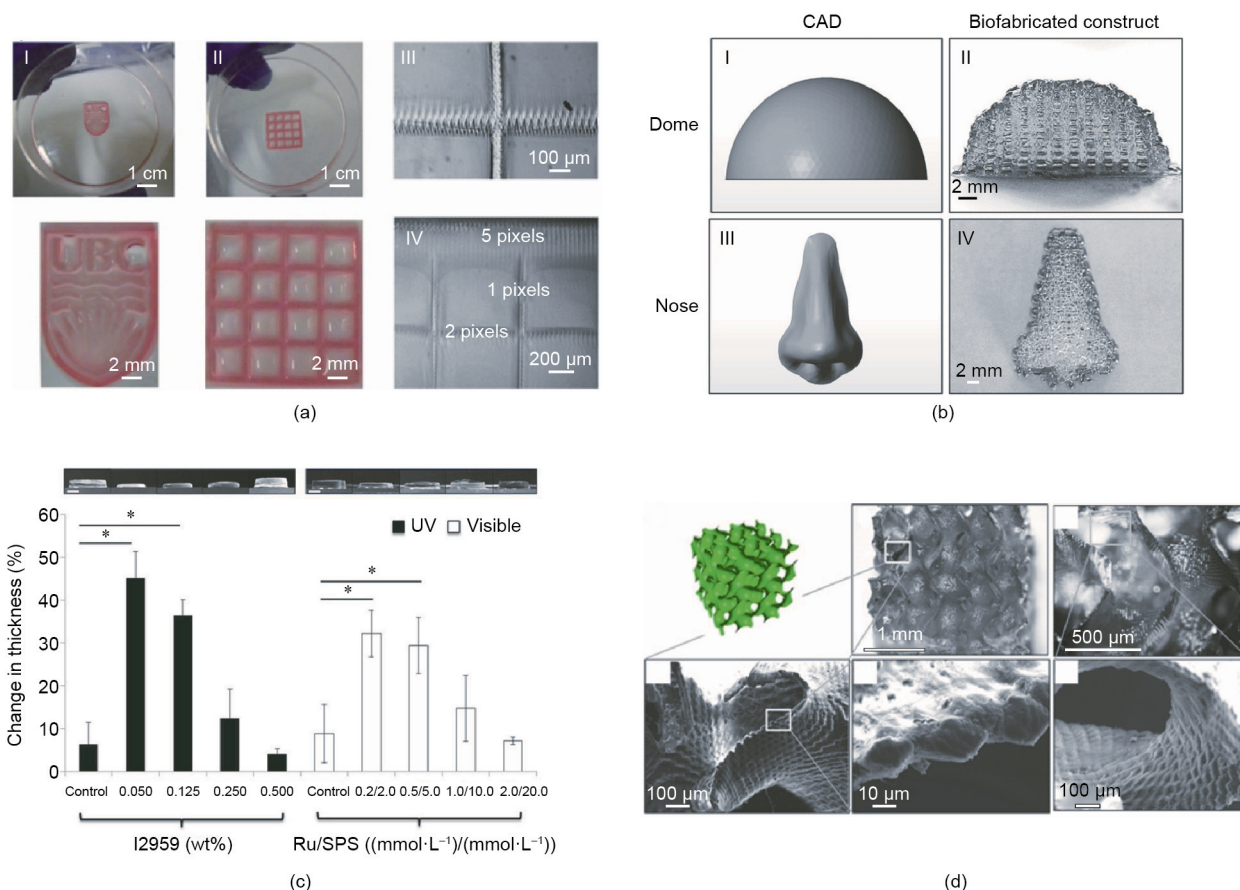
(a)

(b)

(c)

(d)

Fig. 8. (a) Hydrogel patterns fabricated with visible light-induced SLA. (b) Biofabrication of GelMA/Col hydrogel constructs consisting of completely interconnecting 3D pore network. (c) Percentage (%) variation in thickness of GelMA/Col hydrogels with different initiators. Ru: $[Ru(II)(bpy)_3]^{2+}$. (d) Gyroid construct, showing its complex porous pattern. *: $P < 0.05$. CAD: computer aided design. (a) Reproduced from Ref. [26] with permission of IOP Science, © 2015; (b, c) reproduced from Ref. [39] with permission of American Chemical Society, 2016; (d) reproduced from Ref. [27] with permission of IOP Science, © 2019.

vascular tubes. Sakai et al. [33] used $[Ru(II)(bpy)_3]^{2+}$/SPS induced Tyr-modified alginate bioink to print constructs that contain a smooth helical lumen with a diameter of 1 mm. It supplies a solution to construct a complex 3D cell-culture structure containing a vascular network *in vitro*, as shown in Fig. 9(d) [33].

3.4.2. Drug delivery

3D bioprinting, particularly inkjet-based printing, has been used in drug delivery for therapeutic applications. 3D bioprinting offers a viable alternative to traditional tablet manufacturing techniques: Personalized dosage forms customized to the genomic and pathophysiological profile are fabricated. Moreover, it is convenient to design the tablet's shape by bioprinting, so that the drug release can be controlled. Pharmaceutical tablets were made from UV-crosslinked PEGDA and *N*-vinylpyrrolidone (NVP) using 3D inkjet printing to control the release of carvedilol, a drug used to treat hypertension and heart failure [107]. However, UV can affect the stability of active pharmaceutical ingredients. Visible light-induced inkjet bioprinting is a more effective here. Acosta-Vélez et al. [29] used inkjet bioprinting to develop a visible light crosslinkable norbornene-modified HA tablet containing hydrophilic ropinirole, to treat Parkinson's disease and restless legs. Furthermore, ropinirole released 60% within 15 min under acidic condition, which is suitable for oral medicines [29]. Acosta-Vélez et al. [25] developed a PEGDA tablet containing naproxen cured by EY, which controls the release based on the percent of PEGDA in the formulation and the light exposure time for curing the bioinks [25].

4. Conclusion, challenge, and outlook

The expansive field of photopolymerized hydrogel has been researched extensively. In this review, we presented the present status of visible light-curing 3D bioprinting methods and photopolymerized hydrogel initiated by visible light. We summarized the types of initiators and their activation mechanisms. Direct and indirect light-induced strategies ranging from radical polymerization to thiol–ene "click" reaction were investigated. We also reviewed several common biomedical applications of visible light crosslinkable hydrogels in tissue engineering in recent years. Nonetheless, visible light-induced 3D bioprinting systems and the corresponding hydrogels have many more potential areas of application.

During the past several years, considerable progress has been achieved in 3D bioprinting. Given its development potential and application diversity, light-cured 3D bioprinting has been widely researched and is rapidly expanding. The evolution trend of light-cured 3D bioprinting is remarkable. A few common challenges in bioprinting must be addressed. These are with regard to ① printing device, particularly the printing resolution, printing fidelity, and microstructure reproduction; ② cell viability, which involves cellular nutrition and oxygen supply; and ③ bioink property, including the physical strength and biocompatibility. Furthermore, in the area of visible light-induced 3D bioprinting, we must also address the challenge of the photopolymerization speed and print structure fidelity. These can be developed by improving the property of the photopolymerized hydrogels.
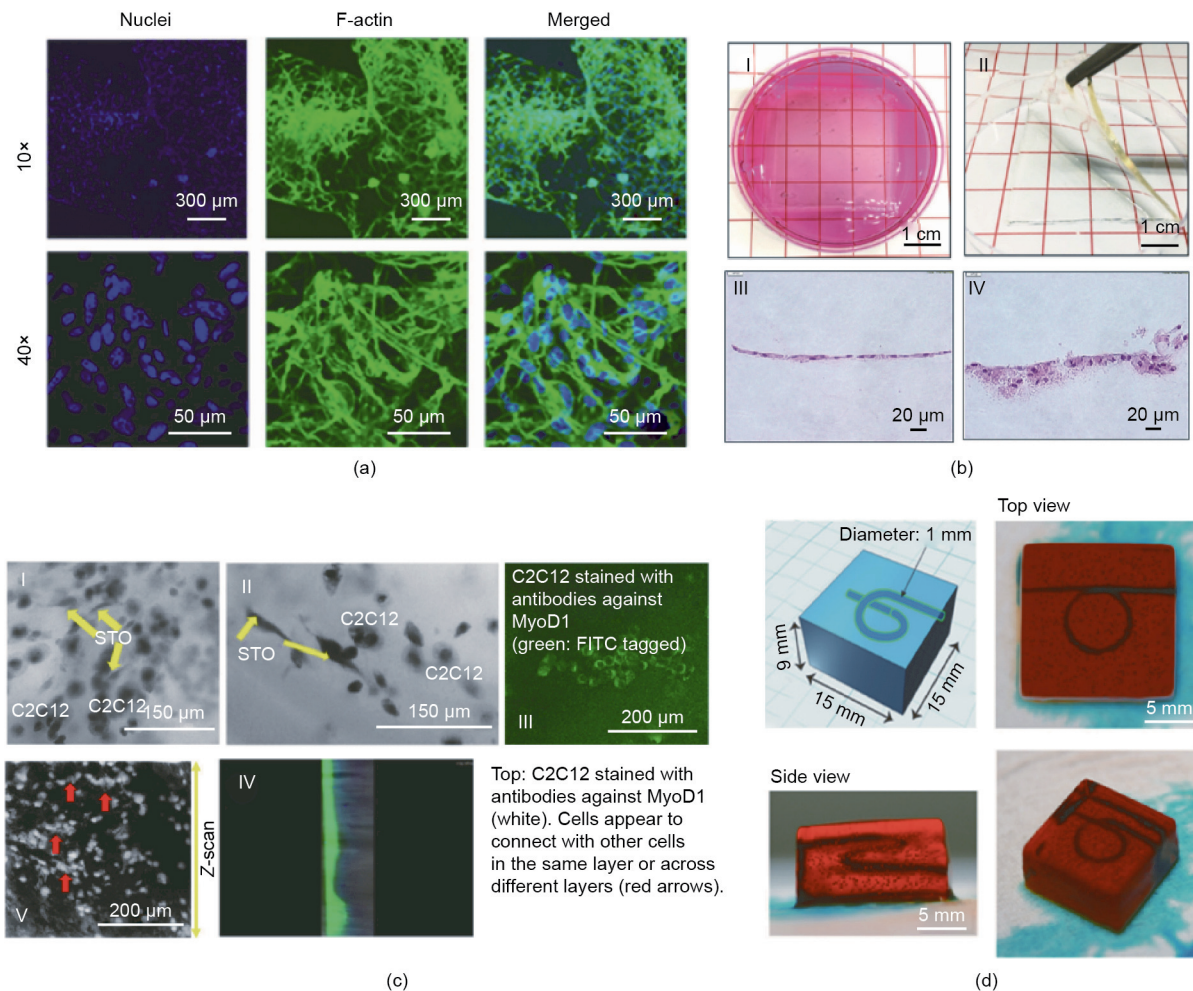
Fig. 9. (a) Confocal fluorescence microscopy images of a junction in 3D-bioprinted cellular networks. (b) Formation of keratin layer on 3D-printed SF/PEG hydrogel containing fibroblast cells. (c) STO fibroblasts cocultured with C2C12 myoblasts cells. MyoD1: myogenic regulatory protein. (d) Blueprint and printed rectangular prism-shaped hydrogel containing a perfusable helical lumen (1 mm in diameter) structure. FITC: fluorescein 5-isothiocyanate. (a) Reproduced from Ref. [103] with permission of American Chemical Society, © 2018; (b) reproduced from Ref. [105] with permission of Elsevier, © 2019; (c) reproduced from Ref. [94] with permission of Wiley, © 2019; (d) reproduced from Ref. [33] with permission of American Chemical Society, © 2018.

Visible light crosslinkable materials exhibit better properties and higher application potential than the photopolymerized hydrogel induced by UV. Although visible light exhibits a lower cytotoxicity than UV light, it has limitations. The activation of the common visible-light initiators generally requires the presence of co-initiators and co-monomers. For example, EY activation requires triethanolamine as a co-initiator and NVP as a co-monomer. Because these are required at relatively high concentrations and because of the co-initiator's cytotoxicity, their application is limited. Research should be performed to overcome this disadvantage by improving the gelation efficiency without increasing the cytotoxicity. One of the methods to solve this problem is to improve the light intensity or mortify the chains with more multifunctional groups. After these challenges are overcome successfully, visible light-induced 3D bioprinting can be integrated effectively into tissue engineering.

Considerable progress has been achieved in 3D bioprinting and tissue engineering in terms of methods and materials. Visible light crosslinkable hydrogels can be photopolymerized as rapidly as UV crosslinkable hydrogels to achieve the appropriate mechanical strength and the desired construct in a spatiotemporal manner. Thereby, these have emerged as versatile biomaterial platforms for 3D bioprinting and tissue engineering. Recent advancements have imparted numerous advantages to visible light crosslinkable hydrogels, such as high cytocompatibility with different types of cells, tunable structure for strength, and cheaper crosslinking device. Moreover, there are many potential application areas for visible light-induced bioprinting, such as disease models and drug screening. The dynamic behavior of cell communication in 3D space can be observed more conveniently *in vitro* by 3D bioprinting than by culturing in a Petri dish. Hydrogel mimics the composition of ECM to accurately simulate dynamic variations *in vivo* as well as the function of natural tissues [78]. In addition, it is more convenient to design and adjust the microstructure of a photopolymerized hydrogel in a spatial layout. Overall, visible light-induced bioprinting has high value for future regenerative and biomedical engineering.

Acknowledgements

Compliance with ethics guidelines

Zizhuo Zheng, David Eglin, Mauro Alini, Geoff R Richards, Ling Qin, and Yuxiao Lai declare that they have no conflict of interest or financial conflicts to disclose.

References

[1] Yan Q, Dong H, Su J, Han J, Song Bo, Wei Q, et al. A review of 3D printing technology for medical applications. Engineering 2018;4(5):729–42.

[2] Zhao P, Gu H, Mi H, Rao C, Fu J, Turng LS. Fabrication of scaffolds in tissue engineering: a review. Front Mech Eng 2018;13(1):107–19.

[3] Lu B, Li D, Tian X. Development trends in additive manufacturing and 3D printing. Engineering 2015;1(1):85–9.

[4] An J, Teoh JEM, Suntornnond R, Chua CK. Design and 3D printing of scaffolds and tissues. Engineering 2015;1(2):261–8.

[5] Kamoun EA, Kenawy ER, Chen X. A review on polymeric hydrogel membranes for wound dressing applications: PVA-based hydrogel dressings. J Adv Res 2017;8(3):217–33.

[6] Farkas B, Dante S, Brandi F. Photoinitiator-free 3D scaffolds fabricated by excimer laser photocuring. Nanotechnology 2017;28(3):034001.

[7] Pereira RF, Bártolo PJ. 3D photo-fabrication for tissue engineering and drug delivery. Engineering 2015;1(1):090–112.

[8] Hull CW, inventor; UVP, Inc, assignee. Apparatus for production of three-dimensional objects by stereolithography. US patents US4575330A. 1986 March 11.

[9] Cui H, Nowicki M, Fisher JP, Zhang LG. 3D bioprinting for organ regeneration. Adv Healthcare Mater 2017;6(1):1601118.

[10] Billiet T, Vandenhaute M, Schelfhout J, Van Vlierberghe S, Dubruel P. A review of trends and limitations in hydrogel-rapid prototyping for tissue engineering. Biomaterials 2012;33(26):6020–41.

[11] Zhang YS, Khademhosseini A. Advances in engineering hydrogels. Science 2017;356(6337):eaaf3627.

[12] Liang R, Wang Li, Yu H, Khan A, Ul Amin B, Khan RU. Molecular design, synthesis and biomedical applications of stimuli-responsive shape memory hydrogels. Eur Polym J 2019;114:380–96.

[13] Li X, Sun Q, Li Q, Kawazoe N, Chen G. Functional hydrogels with tunable structures and properties for tissue engineering applications. Front Chem 2018;6:499.

[14] Brown TE, Anseth KS. Spatiotemporal hydrogel biomaterials for regenerative medicine. Chem Soc Rev 2017;46(21):6532–52.

[15] De la Vega L, Lee C, Sharma R, Amereh M, Willerth SM. 3D bioprinting models of neural tissues: the current state of the field and future directions. Brain Res Bull 2019;150:240–9.

[16] Choi JR, Yong KW, Choi JY, Cowie AC. Recent advances in photo-crosslinkable hydrogels for biomedical applications. Biotechniques 2019;66(1):40–53.

[17] Yao H, Wang J, Mi S. Photo processing for biomedical hydrogels design and functionality: a review. Polymers 2017;10(1):11.

[18] Thakur T, Xavier JR, Cross L, Jaiswal MK, Mondragon E, Kaunas R, et al. Photocrosslinkable and elastomeric hydrogels for bone regeneration. J Biomed Mater Res 2016;104(4):879–88.

[19] Khoshakhlagh P, Bowser DA, Brown JQ, Moore MJ. Comparison of visible and UVA phototoxicity in neural culture systems micropatterned with digital projection photolithography. J Biomed Mater Res 2019;107(1):134–44.

[20] Petta D, Armiento AR, Grijpma D, Alini M, Eglin D, D'Este M. 3D bioprinting of a hyaluronan bioink through enzymatic- and visible light-crosslinking. Biofabrication 2018;10(4):044104.

[21] Zimmermann R, Hentschel C, Schron F, Moedder D, Buettner T, Atallah P, et al. High resolution bioprinting of multi-component hydrogels. Biofabrication 2019;11(4):045008.

[22] Sasaki H, Rothrauff BB, Alexander PG, Lin H, Gottardi R, Fu FH, et al. *In vitro* repair of meniscal radial tear with hydrogels seeded with adipose stem cells and TGF-beta 3. Am J Sports Med 2018;46(10):2402–13.

[23] Hyun H, Park MH, Jo G, Kim SY, Chun HJ, Yang DH. Photo-cured glycol chitosan hydrogel for ovarian cancer drug delivery. Mar Drugs 2019;17(1):41.

[24] Derakhshanfar S, Mbeleck R, Xu K, Zhang X, Zhong W, Xing M. 3D bioprinting for biomedical devices and tissue engineering: a review of recent trends and advances. Bioact Mater 2018;3(2):144–56.

[25] Acosta-Vélez GF, Zhu TZ, Linsley CS, Wu BM. Photocurable poly(ethylene glycol) as a bioink for the inkjet 3D pharming of hydrophobic drugs. Int J Pharm 2018;546(1–2):145–53.

[26] Wang Z, Abdulla R, Parker B, Samanipour R, Ghosh S, Kim K. A simple and high-resolution stereolithography-based 3D bioprinting system using visible light crosslinkable bioinks. Biofabrication 2015;7(4):045009.

[27] Lim KS, Levato R, Costa PF, Castilho MD, Alcala-Orozco CR, van Dorenmalen KMA, et al. Bio-resin for high resolution lithography-based biofabrication of complex cell-laden constructs. Biofabrication 2018;10(3):034101.

[28] Bernal PN, Delrot P, Loterie D, Li Y, Malda J, Moser C, et al. Volumetric bioprinting of complex living-tissue constructs within seconds. Adv Mater 2019;31(42):e1904209.

[29] Acosta-Vélez GF, Linsley CS, Craig MC, Wu BM. Photocurable bioink for the inkjet 3D pharming of hydrophilic drugs. Bioengineering 2017;4(1):11.

[30] Poldervaart MT, Goversen B, de Ruijter M, Abbadessa A, Melchels FPW, Oner FC, et al. 3D bioprinting of methacrylated hyaluronic acid (MeHA) hydrogel with intrinsic osteogenicity. PLoS ONE 2017;12(6):e0177628.

[31] Xu C, Lee W, Dai G, Hong Yi. Highly elastic biodegradable single-network hydrogel for cell printing. ACS Appl Mater Interfaces 2018;10(12):9969–79.

[32] Sakai S, Ohi H, Hotta T, Kamei H, Taya M. Differentiation potential of human adipose stem cells bioprinted with hyaluronic acid/gelatin-based bioink through microextrusion and visible light-initiated crosslinking. Biopolymers 2018;109(2):e23080.

[33] Sakai S, Kamei H, Mori T, Hotta T, Ohi H, Nakahata M, et al. Visible light-induced hydrogelation of an alginate derivative and application to stereolithographic bioprinting using a visible light projector and acid red. Biomacromolecules 2018;19(2):672–9.

[34] Gao G, Yonezawa T, Hubbell K, Dai G, Cui X. Inkjet-bioprinted acrylated peptides and PEG hydrogel with human mesenchymal stem cells promote robust bone and cartilage formation with minimal printhead clogging. Biotechnol J 2015;10(10):1568–77.

[35] Gu BK, Choi DJ, Park SJ, Kim MS, Kang CM, Kim CH. 3-dimensional bioprinting for tissue engineering applications. Biomater Res 2016;20(1):12.

[36] Panwar A, Tan LP. Current status of bioinks for micro-extrusion-based 3D bioprinting. Molecules 2016;21(6):685.

[37] Holzl K, Lin S, Tytgat L, van Vlierberghe S, Gu L, Ovsianikov A. Bioink properties before, during and after 3D bioprinting. Biofabrication 2016;8(3):032002.

[38] Ouyang L, Highley CB, Sun W, Burdick JA. A generalizable strategy for the 3D bioprinting of hydrogels from nonviscous photo-crosslinkable inks. Adv Mater 2017;29(8):1604983.

[39] Lim KS, Schon BS, Mekhileri NV, Brown GCJ, Chia CM, Prabakar S, et al. New visible-light photoinitiating system for improved print fidelity in gelatin-based bioinks. ACS Biomater Sci Eng 2016;2(10):1752–62.

[40] Valot L, Martinez J, Mehdi A, Subra G. Chemical insights into bioinks for 3D printing. Chem Soc Rev 2019;48(15):4049–86.

[41] Zeng Y, Yan Y, Yan H, Liu C, Li P, Dong P, et al. 3D printing of hydroxyapatite scaffolds with good mechanical and biocompatible properties by digital light processing. J Mater Sci 2018;53(9):6291–301.

[42] Deng S, Wu J, Dickey MD, Zhao Q, Xie T. Rapid open-air digital light 3D printing of thermoplastic polymer. Adv Mater 2019;31(39):1903970.

[43] Zhu W, Ma X, Gou M, Mei D, Zhang K, Chen S. 3D printing of functional biomaterials for tissue engineering. Curr Opin Biotechnol 2016;40:103–12.

[44] Kelly BE, Bhattacharya I, Heidari H, Shusteff M, Spadaccini CM, Taylor HK. Volumetric additive manufacturing via tomographic reconstruction. Science 2019;363(6431):1075–9.

[45] Mendes-Felipe C, Oliveira J, Etxebarria I, Vilas-Vilela JL, Lanceros-Mendez S. State-of-the-art and future challenges of UV curable polymer-based smart materials for printing technologies. Adv Mater Technol 2019;4(3):1800618.

[46] Pahoff S, Meinert C, Bas O, Nguyen L, Klein TJ, Hutmacher DW. Effect of gelatin source and photoinitiator type on chondrocyte redifferentiation in gelatin methacryloyl-based tissue-engineered cartilage constructs. J Mater Chem B Mater Biol Med 2019;7(10):1761–72.

[47] Fu A, Gwon K, Kim M, Tae G, Kornfield JA. Visible-light-initiated thiol–acrylate photopolymerization of heparin-based hydrogels. Biomacromolecules 2015;16(2):497–506.

[48] Petta D, Grijpma DW, Alini M, Eglin D, D'Este M. Three-dimensional printing of a tyramine hyaluronan derivative with double gelation mechanism for independent tuning of shear thinning and postprinting curing. ACS Biomater Sci Eng 2018;4(8):3088–98.

[49] Fairbanks BD, Schwartz MP, Bowman CN, Anseth KS. Photoinitiated polymerization of PEG-diacrylate with lithium phenyl-2,4,6-trimethylbenzoylphosphinate: polymerization rate and cytocompatibility. Biomaterials 2009;30(35):6702–7.

[50] Wang Z, Jin X, Dai Ru, Holzman JF, Kim K. An ultrafast hydrogel photocrosslinking method for direct laser bioprinting. RSC Adv 2016;6(25):21099–104.

[51] Nguyen AK, Goering PL, Reipa V, Narayan RJ. Toxicity and photosensitizing assessment of gelatin methacryloyl-based hydrogels photoinitiated with lithium phenyl-2,4,6-trimethylbenzoylphosphinate in human primary renal proximal tubule epithelial cells. Biointerphases 2019;14(2):021007.

[52] Hu J, Hou Y, Park H, Choi B, Hou S, Chung A, et al. Visible light crosslinkable chitosan hydrogels for tissue engineering. Acta Biomater 2012;8(5):1730–8.

[53] Kamoun EA, El-Betany A, Menzel H, Chen X. Influence of photoinitiator concentration and irradiation time on the crosslinking performance of visible-light activated pullulan-HEMA hydrogels. Int J Biol Macromol 2018;120:1884–92.

[54] Donnelly PE, Chen T, Finch A, Brial C, Maher SA, Torzilli PA. Photocrosslinked tyramine-substituted hyaluronate hydrogels with tunable mechanical properties improve immediate tissue–hydrogel interfacial strength in articular cartilage. J Biomater Sci Polym Ed 2017;28(6):582–600.

[55] Al-Abboodi A, Zhang S, Al-Saady M, Ong JW, Chan PPY, Fu J. Printing *in situ* tissue sealant with visible-light-crosslinked porous hydrogel. Biomed Mater 2019;14(4):045010.

[56] Bertlein S, Brown G, Lim KS, Jungst T, Boeck T, Blunk T, et al. thiol–ene clickable gelatin: a platform bioink for multiple 3D biofabrication technologies. Adv Mater 2017;29(44):1703404.

[57] Lin H, Cheng AM, Alexander PG, Beck AM, Tuan RS. Cartilage tissue engineering application of injectable gelatin hydrogel with *in situ* visible-light-activated gelation capability in both air and aqueous solution. Tissue Eng Part A 2014;20(17-18):2402–11.

[58] Greene T, Lin TY, Andrisani OM, Lin CC. Comparative study of visible light polymerized gelatin hydrogels for 3D culture of hepatic progenitor cells. J Appl Polym Sci 2017;134(11):44545.

[59] Gwon K, Kim E, Tae G. Heparin–hyaluronic acid hydrogel in support of cellular activities of 3D encapsulated adipose derived stem cells. Acta Biomater 2017;49:284–95.

[60] Kerscher P, Kaczmarek JA, Head SE, Ellis ME, Seeto WJ, Kim J, et al. Direct production of human cardiac tissues by pluripotent stem cell encapsulation in gelatin methacryloyl. ACS Biomater Sci Eng 2017;3(8):1499–509.

[61] Shoichet MS, Li RH, White ML, Winn SR. Stability of hydrogels used in cell encapsulation: an in vitro comparison of alginate and agarose. Biotechnol Bioeng 1996;50(4):374–81.

[62] Yin J, Yan M, Wang Y, Fu J, Suo H. 3D bioprinting of low-concentration cell-laden gelatin methacrylate (GelMA) bioinks with a two-step cross-linking strategy. ACS Appl Mater Interfaces 2018;10(8):6849–57.

[63] Beck EC, Barragan M, Libeer TB, Kieweg SL, Converse GL, Hopkins RA, et al. Chondroinduction from naturally derived cartilage matrix: a comparison between devitalized and decellularized cartilage encapsulated in hydrogel pastes. Tissue Eng Part A 2016;22(7-8):665–79.

[64] Hoyle C, Bowman C. Thiol–ene click chemistry. Angew Chem Int Ed 2010;49 (9):1540–73.

[65] Zhu H, Yang X, Genin GM, Lu TJ, Xu F, Lin M. The relationship between thiol–acrylate photopolymerization kinetics and hydrogel mechanics: an improved model incorporating photobleaching and thiol–Michael addition. J Mech Behav Biomed Mater 2018;88:160–9.

[66] Hao Y, Lin CC. Degradable thiol–acrylate hydrogels as tunable matrices for three-dimensional hepatic culture: degradable thiol–acrylate hydrogels. J Biomed Mater Res 2014;102(11):3813–27.

[67] Lin CC, Ki CS, Shih H. Thiol–norbornene photoclick hydrogels for tissue engineering applications. J Appl Polym Sci 2015;132(8):41563.

[68] Shih H, Liu HY, Lin CC. Improving gelation efficiency and cytocompatibility of visible light polymerized thiol–norbornene hydrogels via addition of soluble tyrosine. Biomater Sci 2017;5(3):589–99.

[69] Fancy DA, Denison C, Kim K, Xie Y, Holdeman T, Amini F, et al. Scope, limitations and mechanistic aspects of the photo-induced cross-linking of proteins by water-soluble metal complexes. Chem Biol 2000;7(9):697–708.

[70] Loebel C, Broguiere N, Alini M, Zenobi-Wong M, Eglin D. Microfabrication of photo-cross-linked hyaluronan hydrogels by single- and two-photon tyramine oxidation. Biomacromolecules 2015;16(9):2624–30.

[71] Mazaki T, Shiozaki Y, Yamane K, Yoshida A, Nakamura M, Yoshida Y, et al. A novel, visible light-induced, rapidly cross-linkable gelatin scaffold for osteochondral tissue engineering. Sci Rep 2015;4(1):4457.

[72] Kumar SA, Allen SC, Tasnim N, Akter T, Park S, Kumar A, et al. The applicability of furfuryl-gelatin as a novel bioink for tissue engineering applications. J Biomed Mater Res 2019;107(2):314–23.

[73] Tytgat L, Van Damme L, Van Hoorick J, Declercq H, Thienpont H, Ottevaere H, et al. Additive manufacturing of photo-crosslinked gelatin scaffolds for adipose tissue engineering. Acta Biomater 2019;94:340–50.

[74] Yoon SJ, Yoo Y, Nam SE, Hyun H, Lee DW, Um S, et al. The cocktail effect of BMP-2 and TGF-β1 loaded in visible light-cured glycol chitosan hydrogels for the enhancement of bone formation in a rat tibial defect model. Mar Drugs 2018;16(10):351.

[75] Lu M, Liu Yi, Huang YC, Huang CJ, Tsai WB. Fabrication of photo-crosslinkable glycol chitosan hydrogel as a tissue adhesive. Carbohydr Polym 2018;181:668–74.

[76] Chen P, Ning L, Qiu P, Mo J, Mei S, Xia C, et al. Photo-crosslinked gelatin–hyaluronic acid methacrylate hydrogel-committed nucleus pulposus-like differentiation of adipose stromal cells for intervertebral disc repair. J Tissue Eng Regen Med 2019;13(4):682–93.

[77] Gramlich WM, Kim IL, Burdick JA. Synthesis and orthogonal photopatterning of hyaluronic acid hydrogels with thiol–norbornene chemistry. Biomaterials 2013;34(38):9803–11.

[78] Vega SL, Kwon MY, Song KH, Wang C, Mauck RL, Han L, et al. Combinatorial hydrogels with biochemical gradients for screening 3D cellular microenvironments. Nat Commun 2018;9(1):614.

[79] Kim SH, Yeon YK, Lee JM, Chao JR, Lee YJ, Seo YB, et al. Precisely printable and biocompatible silk fibroin bioink for digital light processing 3D printing. Nat Commun 2018;9(1):1620.

[80] Jeon O, Bouhadir KH, Mansour JM, Alsberg E. Photocrosslinked alginate hydrogels with tunable biodegradation rates and mechanical properties. Biomaterials 2009;30(14):2724–34.

[81] Ooi HW, Mota C, ten Cate AT, Calore A, Moroni L, Baker MB. Thiol–ene alginate hydrogels as versatile bioinks for bioprinting. Biomacromolecules 2018;19(8):3390–400.

[82] Stichler S, Jungst T, Schamel M, Zilkowski I, Kuhlmann M, Böck T, et al. Thiol–ene clickable poly(glycidol) hydrogels for biofabrication. Ann Biomed Eng 2017;45(1):273–85.

[83] Cristovão AF, Sousa D, Silvestre F, Ropio I, Gaspar A, Henriques C, et al. Customized tracheal design using 3D printing of a polymer hydrogel: influence of UV laser cross-linking on mechanical properties. 3D Print Med 2019;5(1):12.

[84] Posritong S, Flores Chavez R, Chu TMG, Bruzzaniti A. A Pyk2 inhibitor incorporated into a PEGDA-gelatin hydrogel promotes osteoblast activity and mineral deposition. Biomed Mater 2019;14(2):025015.

[85] Lin H, Beck AM, Shimomura K, Sohn J, Fritch MR, Deng Y, et al. Optimization of photocrosslinked gelatin/hyaluronic acid hybrid scaffold for the repair of cartilage defect. J Tissue Eng Regen Med 2019;13(8):1418–29.

[86] Campiglio CE, Contessi Negrini N, Fare S, Draghi L. Cross-linking strategies for electrospun gelatin scaffolds. Materials 2019;12(15):2476.

[87] Van Den Bulcke AI, Bogdanov B, De Rooze N, Schacht EH, Cornelissen M, Berghmans H. Structural and rheological properties of methacrylamide modified gelatin hydrogels. Biomacromolecules 2000;1(1):31–8.

[88] Liang X, Wang X, Xu Qi, Lu Y, et al. Rubbery chitosan/carrageenan hydrogels constructed through an electroneutrality system and their potential application as cartilage scaffolds. Biomacromolecules 2018;19(2):340–52.

[89] Cheng YL, Chen F. Preparation and characterization of photocured poly (ε-caprolactone) diacrylate/poly (ethylene glycol) diacrylate/chitosan for photopolymerization-type 3D printing tissue engineering scaffold application. Mater Sci Eng C 2017;81:66–73.

[90] Toole BP. Hyaluronan: from extracellular glue to pericellular cue. Nat Rev Cancer 2004;4(7):528–39.

[91] Suo A, Xu W, Wang Y, Sun T, Ji L, Qian J. Dual-degradable and injectable hyaluronic acid hydrogel mimicking extracellular matrix for 3D culture of breast cancer MCF-7 cells. Carbohydr Polym 2019;211:336–48.

[92] Highley CB, Prestwich GD, Burdick JA. Recent advances in hyaluronic acid hydrogels for biomedical applications. Curr Opin Biotechnol 2016;40:35–40.

[93] Hinton TJ, Jallerat Q, Palchesko RN, Park JH, Grodzicki MS, Shue HJ, et al. Three-dimensional printing of complex biological structures by freeform reversible embedding of suspended hydrogels. Sci Adv 2015;1(9):e1500758.

[94] Inoue S, Tanaka K, Arisaka F, Kimura S, Ohtomo K, Mizuno S. Silk fibroin of Bombyx mori is secreted, assembling a high molecular mass elementary unit consisting of H-chain, L-chain, and P25, with a 6:6:1 molar ratio. J Biol Chem 2000;275(51):40517–28.

[95] Shi L, Wang F, Zhu W, Xu Z, Fuchs S, Hilborn J, et al. Self-healing silk fibroin-based hydrogel for bone regeneration: dynamic metal-ligand self-assembly approach. Adv Funct Mater 2017;27(37):1700591.

[96] Lee KY, Mooney DJ. Alginate: properties and biomedical applications. Prog Polym Sci 2012;37(1):106–26.

[97] Chaicharoenaudomrung N, Kunhorm P, Promjantuek W, Heebkaew N, Rujanapun N, Noisa P. Fabrication of 3D calcium-alginate scaffolds for human glioblastoma modeling and anticancer drug response evaluation. J Cell Physiol 2019;234(11):20085–97.

[98] Hasan Shahriari M, Shokrgozar MA, Bonakdar S, Yousefi F, Negahdari B, Yeganeh H. In situ forming hydrogels based on polyethylene glycol itaconate for tissue engineering application. Bull Mater Sci 2019;42(4):193.

[99] Hao Y, Shih H, Muñoz Z, Kemp A, Lin CC. Visible light cured thiol–vinyl hydrogels with tunable degradation for 3D cell culture. Acta Biomater 2014;10(1):104–14.

[100] Li H, Zheng H, Zhang Y, Zhang W, Tong W, Gao C. Preparation of photo-responsive poly(ethylene glycol) microparticles and their influence on cell viability. J Colloid Interface Sci 2018;514:182–9.

[101] Liang J, Guo Z, Timmerman A, Grijpma D, Poot A. Enhanced mechanical and cell adhesive properties of photo-crosslinked PEG hydrogels by incorporation of gelatin in the networks. Biomed Mater 2019;14(2):024102.

[102] Bal T, Nazli C, Okcu A, Duruksu G, Karaöz E, Kizilel S. Mesenchymal stem cells and ligand incorporation in biomimetic poly(ethylene glycol) hydrogels significantly improve insulin secretion from pancreatic islets. J Tissue Eng Regen Med 2017;11(3):694–703.

[103] Wang Z, Kumar H, Tian Z, Jin X, Holzman JF, Menard F. Visible light photoinitiation of cell-adhesive gelatin methacryloyl hydrogels for stereolithography 3D bioprinting. ACS Appl Mater Interfaces 2018;10(32):26859–69.

[104] Galarraga JH, Kwon MY, Burdick JA. 3D bioprinting via an in situ crosslinking technique towards engineering cartilage tissue. Sci Rep 2019;9(1):19987.

[105] Kwak H, Shin S, Lee H, Hyun J. Formation of a keratin layer with silk fibroin–polyethylene glycol composite hydrogel fabricated by digital light processing 3D printing. J Ind Eng Chem 2019;72:232–40.

[106] Kumar SA, Alonzo M, Allen SC, Abelseth L, Thakur V, Akimoto J, et al. A visible light-cross-linkable, fibrin–gelatin-based bioprinted construct with human cardiomyocytes and fibroblasts. ACS Biomater Sci Eng 2019;5(9):4551–63.

[107] Clark EA, Alexander MR, Irvine DJ, Roberts CJ, Wallace MJ, Yoo J, et al. Making tablets for delivery of poorly soluble drugs using photoinitiated 3D inkjet printing. Int J Pharm 2020;578:118805.